Contrib Mineral Petrol (1982) 81:253–261

Contributions to Mineralogy and Petrology

Distribution of the Glass Phase in Hot-Pressed, Olivine-Basalt Aggregates: An Electron Microscopy Study

P.J. Vaughan* and D.L. Kohlstedt
Department of Materials Science and Engineering Cornell University Ithaca, New York 14853, USA
H.S. Waff, Department of Geology, University of Oregon, Eugene, Oregon 97403, USA

Abstract. Samples of olivine mixed with small amounts of tholeiitic basalt which were hot-pressed above the solidus temperature were examined by transmission electron microscopy (TEM) and scanning electron microscopy (SEM) techniques. Two sets of samples were compared. One set was hot-pressed for approximately 1 h near 1,300° C at 0.2 GPa, and the other set was held for approximately 200 h near 1,250° C at 1.0 GPa. SEM observations reveal that, in samples which were hot-pressed for 1 h, the glass phase occurs in irregular pockets surrounded by four or five olivine grains as well as in triple junctions. The crystal-glass interfaces show both positive and negative curvature. These observations and the presence of voids suggest that the microstructure is far from textural equilibrium. In contrast, in samples which were hot-pressed for 200 h, glass is largely confined to triple junctions of uniform size and the crystal-glass interfaces have uniform curvature indicating a much greater degree of textural equilibrium. TEM images reveal layers of glass 10–50 nm thick along most of the grain boundaries in the samples annealed for short times. However, within the limit of resolution, ~2 nm, virtually all of the grain boundaries in the samples hot-pressed for long times appear to contain no glass. These observations indicate that segregation of melt from grain boundaries to triple junctions is an integral part of the process of textural equilibration.

Introduction

The distribution of melt at the scale of individual grains markedly affects the physical properties of partially melted rocks. For example, if the melt forms an interconnected network, electrical conductivity can be several orders of magnitude greater than in unmelted rocks. Mass transport in the liquid phase is generally much faster than through melt-free grain boundaries. A solution-precipitation mechanism could augment mechanisms of creep such as grain-boundary sliding and dislocation flow. A wetting melt can markedly increase the elastic compliance and seismic attenuation (internal friction) of rocks. In contrast, a small percentage of liquid in isolated pockets has little influence on these physical properties.

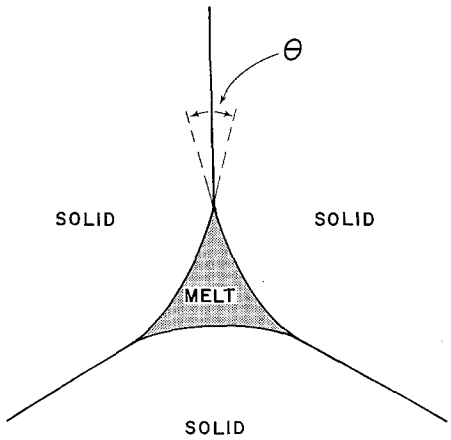

Fig. 1. Schematic diagram of a triple junction containing melt and bounded by three solid grains. The angle θ is the dihedral angle

To determine possible solid-melt microstructures in the earth's upper mantle, Waff and Bulau (1979) examined partially melted olivine plus basalt mixtures with optical and scanning electron (SEM) microscopes. Within the resolution of these instruments (~20 nm, SEM) no melt was detected in two-grain junctions, hereafter simply called grain boundaries. Glass (quenched melt) was, however, observed in all three-grain junctions which were examined. The authors concluded that the network of melt was interconnected only along channels formed by the edges of three grains (i.e., triple junctions), as illustrated in Fig. 1.

To extend the observations on melt distribution to substantially higher resolution, we have examined partially melted samples of olivine plus basalt with the transmission electron microscope (TEM). High-resolution TEM techniques have recently been used to determine the presence or absence of very thin (<2 nm) intergranular films of glass in ceramic materials (for a review, see Clarke 1979). Many commercially important ceramic materials are fabricated by liquid-phase sintering in order to obtain, at moderate temperatures, high-density polycrystalline structural ceramics from phases with very high melting temperatures. For example, silicon nitride is frequently hot-pressed or sintered with small amounts of magnesia or yttria. As with partial melts in rocks, a continuous, microscopic grain-boundary layer of a melt phase can strongly influence macroscopic properties.

* *Present address:* Now at Department of Geology, University of California, Davis, USA

Experimental Details

Specimen Preparation

Specimens of olivine plus basalt were prepared by isostatically hot-pressing a mechanical mixture of powders of olivine plus basalt above the solidus temperature. One series of samples was pressed at relatively low pressures for short times, and a second series was pressed at high pressures for long times.

High-Pressure, Long-Time Specimens. Two samples were prepared by Waff and Bulau (1979) at 1 GPa in a solid-medium high-pressure apparatus. Starting powders smaller than 250 μm were ground from a dunite xenolith from Hualailai, Hawaii, and Picture Gorge basalt. The powders were sealed into Pt capsules. Sample WB#5 containing 5 wt.% basalt was held at 1,245° C for 165 h. Sample WB#8 with 1.6 wt.% basalt was isostatically pressed at 1,245° C for 222 h.

Low-Pressure, Short-Time Specimens. The first group of samples, IHP#1, were prepared from powders of San Carlos olivine plus 5 wt.% Hawaiian tholeiitic basalt. Powders, prepared by grinding in a shatterbox, were sorted according to particle size in an air classifier. The particle size of the basalt powder was less than 10 μm and the particle size of the olivine powder was in the range of 10 to 15 μm. The two types of powders were mixed together in the shatterbox. The powders were sealed by electron beam welding in thin-walled Pd capsules approximately 15 mm long and 5 mm in diameter. Samples were held for 1 h at 1,275° C at 225 MPa in our gas high-pressure apparatus.

A second group of samples, IHP#2, were prepared from the same tholeiitic Hawaiian basalt and Balsam Gap dunite. The powders were again ground and mixed in a shatterbox. The particle size of the sieved dunite powder was less than 44 μm. The mixture was sealed in thick-walled (2 mm) Fe jackets by heliarc welding. Samples approximately 2 cm long and 5 cm in diameter were isostatically hot-pressed commercially at 1,350° C for 4 h under 200 MPa gas pressure.

Imaging Conditions

TEM foils were prepared from polished, 30 μm-thick thin sections of samples of olivine plus basaltic melt. Pieces of the thin section approximately 2 mm across were mounted between copper washers and ion-thinned to perforation. The thinned samples were carbon coated before examination on a Siemens 102 electron microscope operating at 125 kV. Three TEM techniques were used in this study. The imaging conditions are described below.

Lattice-Fringe Images. Edge-on or nearly edge-on grain boundaries were examined by the bright-field lattice-fringe imaging technique (Cowley 1975; Clarke 1979). The TEM foils were tilted until the Bragg condition was satisfied for at least one set of lattice planes in each of the two neighboring grains. The objective aperture was placed to include the transmitted and the diffracted beams as shown in Fig. 2. In practive, lattice-fringe images could be obtained in both grains simultaneously only with the (020) planes. The (020) reflection produces the largest fringe spacing, 0.51 nm

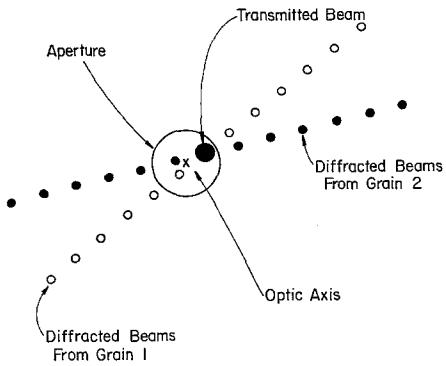

Fig. 2. Schematic diagram of diffraction conditions and aperture position used to form lattice fringe images in two adjacent grains

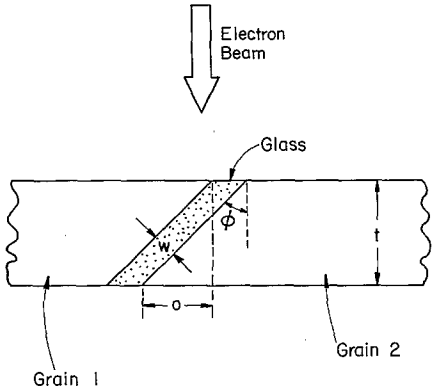

Fig. 3. Schematic diagram of TEM foil containing a glass layer which is inclined to the electron beam

(5.1 Å), for the olivine lattice. (The (010) reflection is forbidden for the Pbmn space group, but due to double diffraction it is often present in diffraction patterns and yields a fringe spacing of 1.02 nm). To maximize resolution, tilted illumination was used such that the transmitted and diffracted beams were equally disposed about the optic axis of the microscope (Edington 1976, pp. 16, 185). The defocus of the objective and condenser lenses was adjusted to give the sharpest lattice-fringe images.

The lattice-fringe imaging technique can be used to detect grain-boundary films of glass of a few tenths of a nanometer provided that the boundary is exactly edge-on. If the boundary is slightly inclined to the electron beam, the overlap of the two grains will decrease the resolution of this technique (Lou et al. 1978; Clark 1979). From geometric considerations, in Fig. 3 the width, w, of a glass layer in a grain boundary inclined at an angle Φ to the electron beam must be greater than t tan Φ (i.e., $w > t \tan \Phi$) if the glass is to be observed in a TEM foil of thickness t. Thus, for example, a grain boundary must be oriented to an accuracy of at least 2° in order to observe an amorphus layer of 1 nm width in a foil which is 30 nm thick. In addition, the objective lens (i.e., the image) must be somewhat underfocused to attain the maximum resolution (Krivanek et al. 1979).

Diffuse-Scattering Images. Dark-field images were formed with the diffusely scattered electrons which come from the amorphous regions within the glass/solid microstructure (Rühle et al. 1977; Krivanek et al. 1979). The diffuse ring

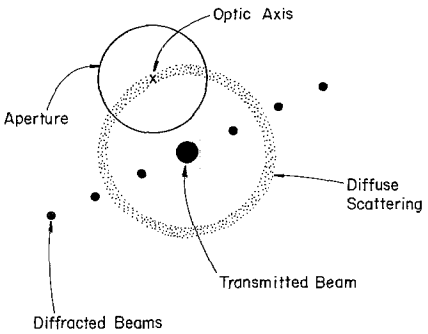

Fig. 4. Schematic diagram of diffraction condition and aperture position used to form an image with diffusely scattered electrons

around the transmitted beam, illustrated in Fig. 4, could be seen only when the selected area diffraction aperture contained a large percentage (>30%) glass; that is, it was visible in diffraction patterns taken from triple junctions and was not visible in diffraction patterns from grain boundaries. As illustrated in Fig. 4, the objective aperture was positioned to include a portion of the diffuse ring (i.e., electron scattering from the glass) and to exclude all Bragg reflections (i.e., scattering from the crystalline grains).

The resolution of the diffuse scattering images is better than 1 nm. Unlike the lattice-fringe images, images formed using the diffusely scattered intensity are relatively insensitive to the inclination of the boundary to the electron beam and to the defocus of the microscope (Krivanek et al. 1979).

Phase-Contrast Images. A series of bright-field micrographs was recorded in which the focus of the objective lens was incrementally varied from an under-focus to an over-focus condition. In under-focus images recorded with this phase-contrast technique, a grain boundary containing glass will appear as a bright band delineated by a pair of alternating dark and bright defocus or Fresnel (Edington 1976, p. 6) fringes. The intensity of the Fresnel fringes decreases rapidly with increasing distance from the interface. In over-focus images, the contrast will be reversed (Clarke 1979, 1980). If a grain boundary does not contain glass, two situations are possible. First, if the inner potentials for the neighboring grains are the same (i.e., independent of the orientations of the grains with respect to the incident electron beam), then the Fresnel fringes will be absent. If the inner potential changes on crossing the grain boundary (due to the change in orientation), a single set of Fresnel fringes should be present. This technique is analogous to the Becke-line method used in optical crystallography to determine the index of refraction of transparent materials (Bloss 1961).

The resolution of the phase-contrast method is <1 nm. The main advantage of this technique compared to the lattice-fringe imaging technique is that the grain boundary need not be oriented precisely parallel to the electron beam in order to detect a very thin layer of glass.

Results

High-Pressure, Long-Time Samples

Optical and SEM micrographs of one of the samples, WB#8, isostatically hot-pressed at 1 GPa have been published by Waff and Bulau (1979). The microstructure in the samples annealed for long times at high pressure appears to be at or, at least, very close to textural equilibrium determined by the relative solid-solid, solid-liquid grain boundary energies (Kingery et al. 1976, p. 212). The melt is quite homogeneously distributed and is largely located at triple junctions. Grain boundaries meet at angles of approximately 120°. No melt was observed in the grain boundaries. SEM observations made as part of the present study also demonstrated that no glass could be resolved in the grain boundaries by this technique; this result places an upper limit of ~10 nm on the width of a glass layer which could be present in the grain boundaries. Electron microprobe analyses revealed no difference in chemistry between the matrix and grain boundaries, supporting this 10 nm upper limit.

To complement and extend the resolution of the SEM observations, the glass-olivine microstructure has been examined using high-resolution TEM techniques.

Lattice-Fringe Images. The major difficulty in using the lattice-fringe imaging technique to detect very thin layers of glass separating two crystalline grains is in orienting the grain boundary parallel to the electron beam and simultaneously obtaining lattice-fringe images in both grains. If the grain boundary is slightly inclined to the electron beam so that the projected images of the two grains overlap. Moiré fringes (Edington 1976, pp. 188–192) will be observed in the vicinity of the grain boundary. This situation is demonstrated clearly in Fig. 5a. The angle, β, between the (020) lattice planes in the grain on the left and those in the grain on the right is 30°. The spacing between the Moiré fringes, D, is 1.02 nm, in good agreement with the value calculated from the relation $D=(d/2\sin(\beta/2))$ where $d=0.51$ nm is the spacing between the (020) lattice fringes. The set of Moiré fringes varies in width from ~4 nm to ~8 nm, indicating that the inclination of the boundary to the electron beam varies along the length of the boundary. For such an inclined grain boundary, it is impossible to detect a thin layer of glass with the lattice fringe imaging technique. In Fig. 5b, which is a lattice-fringe image of another portion of the grain boundary shown in Fig. 5a, steps (ledges) and a set of Moiré fringes of varying width are present. Thus, this ribbon-like grain boundary has curvature both in the direction of the electron beam and along the trace of the boundary.

Although a small fraction of the grain boundaries contain relatively wide, 10–50 nm, layers of glass, most of the grain boundaries examined by the lattice-fringe imaging technique appeared to be free of glass. An example is presented in Fig. 5c. For at least small segments of this grain boundary, no Moiré fringes are visible indicating that the boundary is nearly vertical. In these regions, if glass is present, the glass layer must be less than 2 nm in width. Similar regions are also marked in Fig. 5b.

Diffuse-Scattering Images. To provide a lower magnification view of the solid-glass microstructure, triple junctions and grain boundaries in the vicinity of triple junctions were examined by the diffuse-scattering technique. In Fig. 6, which is a micrograph recorded with the diffusely scattered intensity, glass in the triple junction appears bright and the three bounding crystalline grains are dark. The dark elliptical region within the triple junction is a hole produced by the ion thinning process. Each crystalline grain is misoriented from the neighboring two grains by >20°.

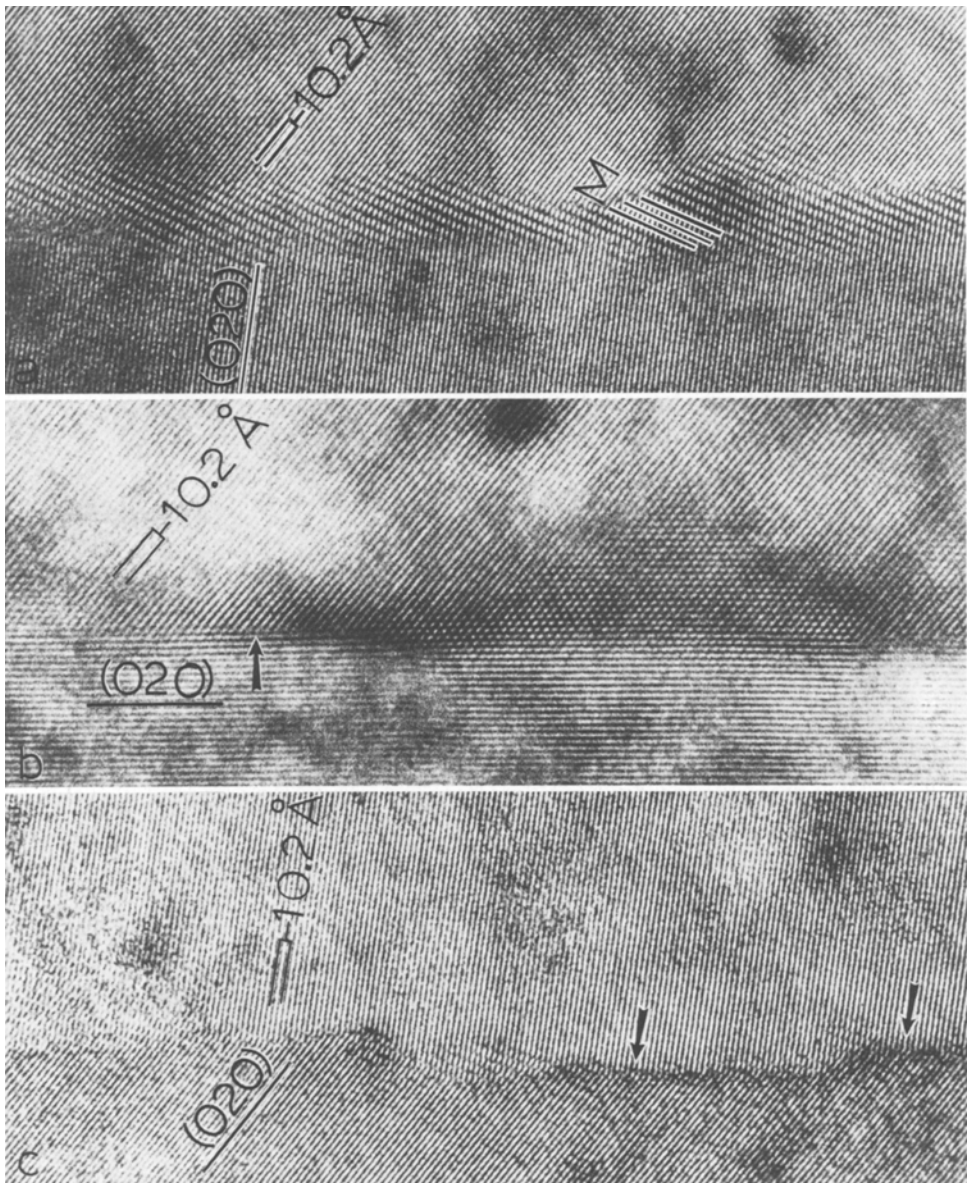

Fig. 5a–c. Lattice-fringe images of the (020) planes in two adjacent olivine grains in a specimen annealed under 1 GPa confining pressure.
a Moiré fringes, labeled *M*, are present because the boundary between the two grains is inclined to the electron beam.
b and **c** In regions marked by *arrows*, Moiré fringes are very short or absent along portions of the grain boundary indicating that it is near vertical. No glass layer is observed in these boundaries

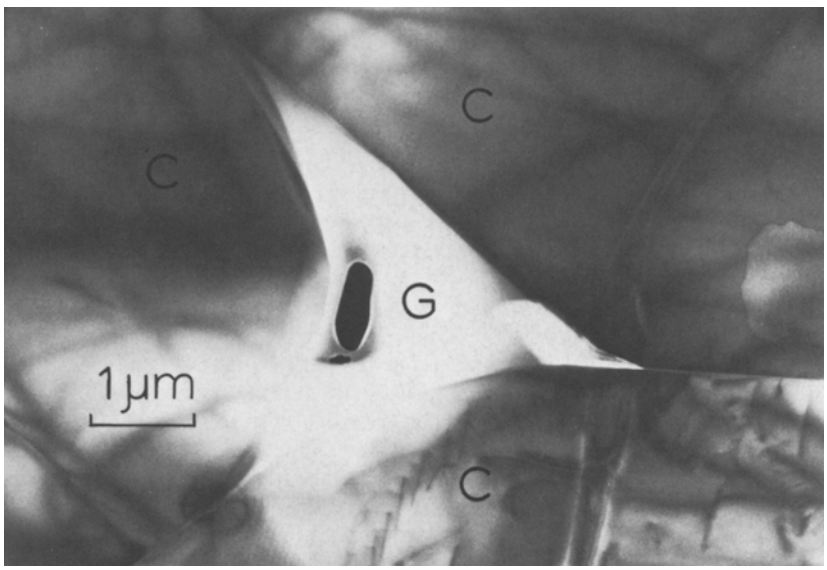

Fig. 6. Dark-field micrograph of a triple junction containing glass in a specimen annealed at 1 GPa. The glass, *G*, appears bright relative to the crystalline grains, *C*, in this micrograph because the image was formed with electrons scattered from the glass as shown in Fig. 4. The small, black region in the glass is a hole which was produced during ion thinning

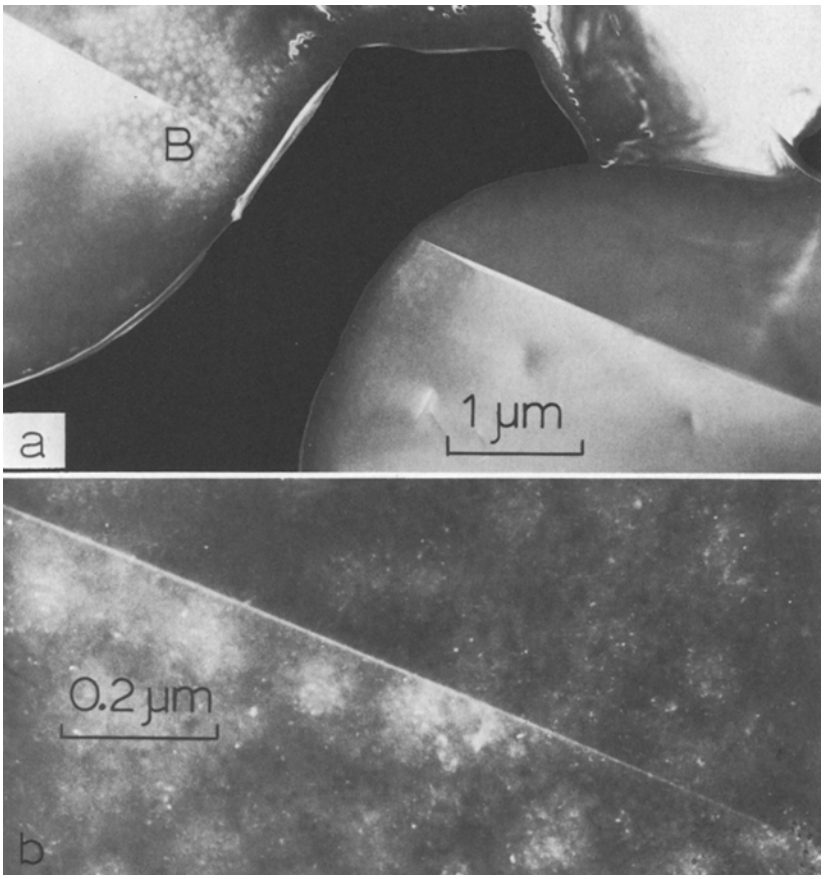

Fig. 7a, b. Image formed with diffusely scattered electrons showing a grain boundary trending NW-SE in a specimen annealed at 1 GPa. The black area in (**a**) is a hole produced by ion thinning. Region *B* in (**a**) is imaged at higher magnification in (**b**) in order to reveal a band ~10 nm wide of high intensity along the boundary

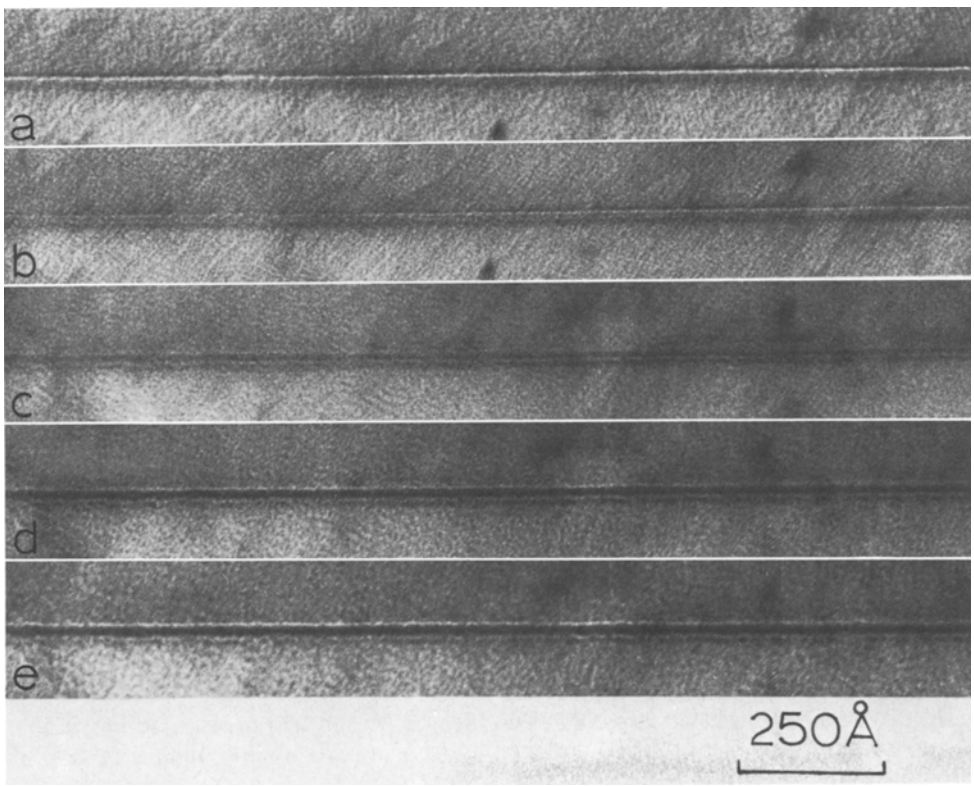

Fig. 8a–d. Through-focus series of bright-field micrographs of boundary between two olivine grains in a specimen annealed at 1 GPa.
a 640 nm under focus,
b 320 nm under focus,
c near focus,
d 320 nm over focus, and
e 640 nm over focus. If a glass layer is present, its maximum thickness is 1 nm, which is the spacing between Fresnel fringes in (**c**) the near-focus image

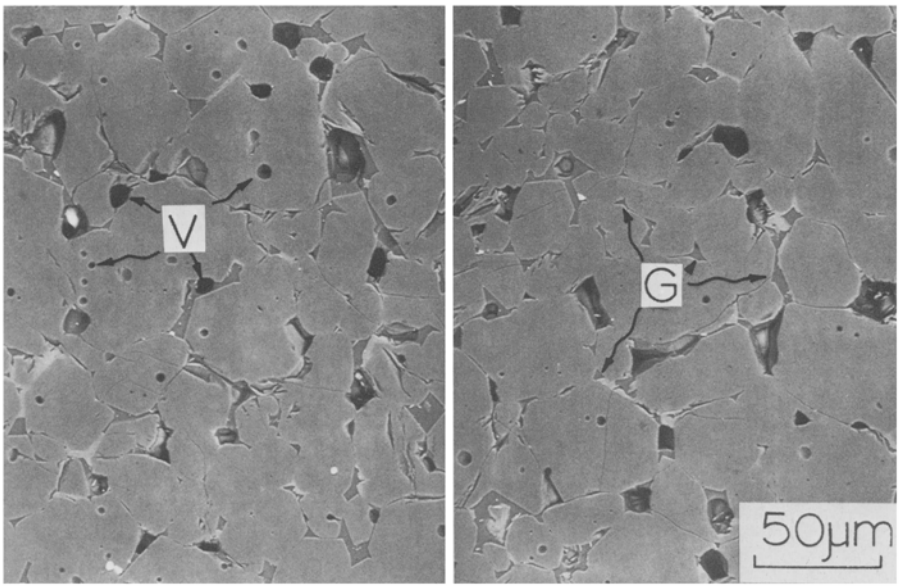

Fig. 9. Backscattered SEM image of basalt-olivine distribution in sample IHP#2 which was prepared at 200 MPa confining pressure. Voids, V, and glass pockets, *G* are noted

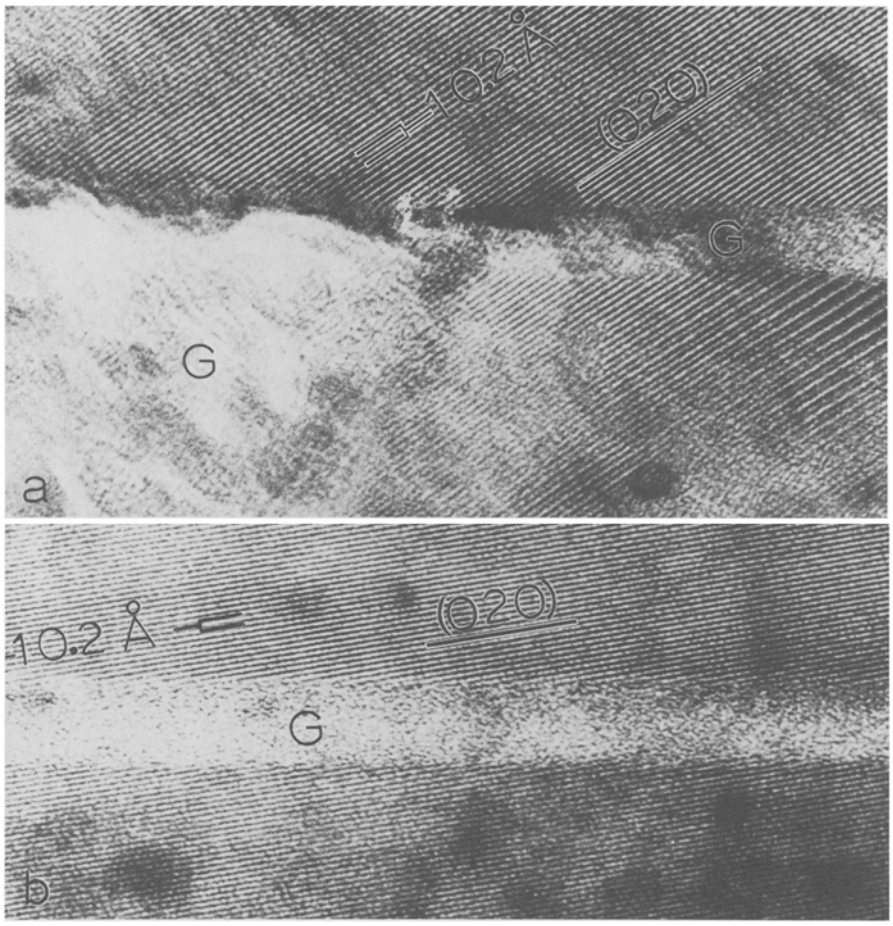

Fig. 10a, b. Lattice-fringe image of two pieces of an olivine grain, in sample IHP #1, separated by a fracture which is filled with glass, *G*. Note that the (020) lattice fringes are parallel in the two halves of the grain.
a Glass extends from a triple junction into the fracture.
b A region several microns from a triple junction

In diffuse-scattering images, almost every grain boundary appeared as a narrow, $\lesssim 10$ nm, wide band of bright intensity. As an example of this observation, the region labeled B of the high-angle ($>30°$) grain boundary in Fig. 7a is shown at higher magnification in Fig. 7b. The presence of the bright band suggests the possibility that virtually all grain boundaries in the olivine-basalt samples contain melt, a result which would be in conflict with the results reported above from the lattice-fringe images. To resolve this apparent contradiction, the grain boundary in Fig. 7 was further examined with standard phase-contrast images.

Phase-Contrast Images. A through-focus series of bright-field micrographs from area B of the grain boundary in Fig. 7a is presented in Fig. 8. The focus condition was

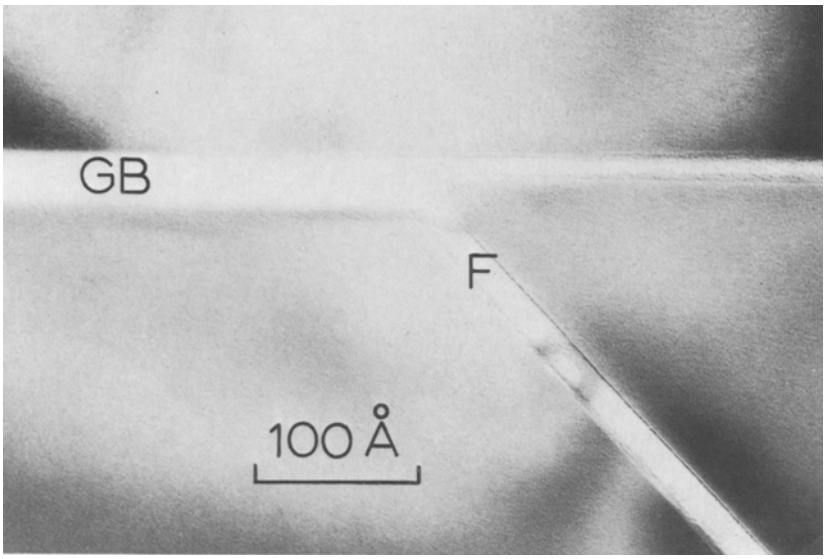

Fig. 11. Bright-field micrograph of a fracture, *F*, in sample IHP #1 which contains glass intersecting a grain boundary, *GB*, which also contains glass. This microstructure suggests that, at least, in some grain boundaries, glass was injected upon fracturing during cooling

changed by 320 nm between micrographs. Figure 8a is under-focused by 640 nm; Fig. 8c is near focus; and Fig. 8e is over-focused by 640 nm.

Fresnel fringes are clearly present in the vicinity of the grain boundary. There appear to be only a single set of fringes. In the under-focus case (Fig. 8a), a traverse from the upper grain to the lower grain crosses first a dark fringe and then a bright fringe. The contrast is reversed in the overfocus case. Near the focus condition, the width of the region in which fringes can be observed is ~ 1 nm. Thus, if a layer of glass is present in the grain boundary, it must be $\lesssim 1$ nm in width.

Low-Pressure, Short-Time Specimens

SEM Observations. A SEM micrograph showing an overview of the microstructure of one of the samples isostatically hot-pressed at low hydrostatic pressure, IHP#2, is presented in Fig. 9. The low-pressure samples are approximately 85% dense. The microstructure indicates that these samples are not in textural equilibrium. The melt is distributed inhomogeneously. While some triple junctions contain very little glass, large pockets of glass often separate as many as five crystalline grains, rather than three grains as expected in equilibrium. Crystal-glass interfaces with negative as well as positive radii of curvature are common.

The difficulty in resolving very narrow glass layers with the SEM is illustrated in Fig. 9. Glass can be observed extending for some distance from triple junctions into grain boundaries. It is seldom possible to follow a glass layer from one triple junction to the next. Such grain boundaries may indeed be free of glass; however, the SEM does not provide resolution of better than approximately ten nanometers.

TEM Observations. Microcracks such as those shown in Fig. 10, are common features in partially melted olivine-basalt samples. A lattice-fringe image of a thin layer of glass extending from a triple junction into a microcrack is presented in Fig. 10a. Diffraction patterns from the material in the triple junction contain only the transmitted beam and a diffuse ring, demonstrating that this material is amorphous. Because the material in the grain boundary is continuous with the glass in the triple junction, the grain boundary must be filled with glass, also. Glass separating two halves of a fractured grain several microns from a triple junction is shown in Fig. 10b. In both cases, the (020) lattice fringes in one crystalline region, although interrupted by the layer of glass, are parallel to those in the other crystalline region. Thus, the two crystalline areas have the same crystallographic orientation and must have been parts of the same grain.

Glass was readily visible under conventional bright-field conditions in many of the grain boundaries in the low-pressure samples. In Fig. 11, a fracture, which is filled with glass, intersects a grain boundary which is also filled with glass. The width of the glass layer changes discontinuously from ~ 4 nm to < 2 nm at the point at which the fracture intersects the grain boundary.

Other grain boundaries, however, appear to be free of glass. For example, in Fig. 12a and b the (020) lattice fringes from one grain terminate in apparent contact with the (020) lattice fringes from the neighboring grain. In Fig. 12a, the angle between the two sets of fringes is $\sim 148°$. A close examination of this micrograph in the vicinity of the grain boundary reveals a series of Moiré fringes approximately 3 nm wide at an angle of $\sim 30°$ to the grain boundary. As discussed in reference to Fig. 5, the Moiré fringes demonstrate that the projected images of the two grains overlap slightly; that is, the grain boundary is inclined at a small angle to the electron beam. An upper limit can be placed on the thickness of a possible glass layer in the grain boundary. From Fig. 3, $w = t \sin\theta - O \cos\theta$. The grain boundary is oriented within 10° of the vertical and $t \simeq 30$ nm. Thus, $w \leqq 2$ nm.

Discussion

Glass is present in many of the grain boundaries in the samples hot-pressed at low pressures for short times (Figs. 10 and 11). These samples contain approximately 15% porosity; the melt is inhomogeneously distributed; and grain boundaries often do not meet at 120° angles (Fig. 9). Elongated wedges of glass penetrate deeply from

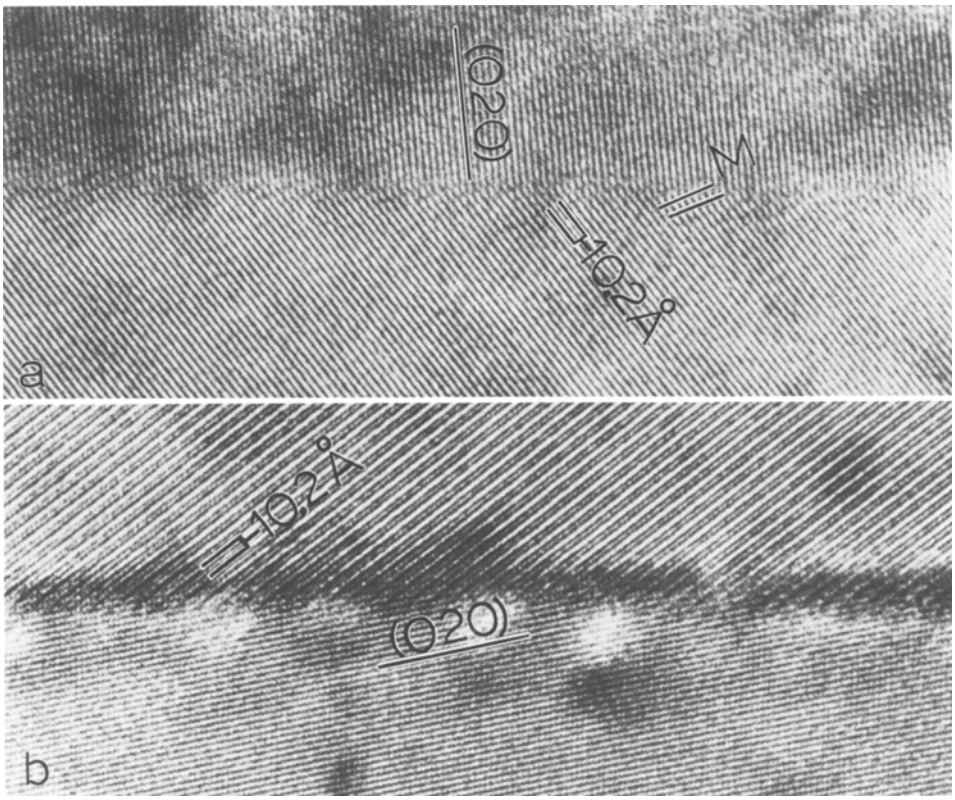

Fig. 12a, b. Lattice-fringe image of two olivine grains in sample IHP #2.
a The (020) lattice fringes are imaged in both grains. Moiré fringes, *M*, ~3 nm wide are noted.
b The (020) lattice fringes are imaged in the lower grain, while the (010) fringes dominate in the upper grain. The fringes from the two grains overlap by ~2 nm

some triple junctions into grain boundaries in which no glass was observed far from the triple junctions. This geometry suggests that melt is being expelled from the grain boundary into the triple junction. Thus, the melt-solid microstructure has not yet attained a textural equilibrium controlled by the solid-liquid and solid-solid surface energies.

In contrast, virtually all of the grain boundaries which we examined in the samples prepared near 1 GPa and 1,250° C for more than 150 h appear to be free of glass (Figs. 4 and 5). The orientation of a grain boundary varies along the boundary. In sections of these grain boundaries which are vertical or nearly vertical, lattice fringes in one grain contact the lattice fringes in the neighboring grain. These grain boundaries appear to contain no glass. *If* glass is present in these boundaries, the glass layer is apparently less than 2 nm thick. In the few boundaries in which glass was observed, the glass layer was quite wide, 10–50 nm. These boundaries may have fractured during quenching to allow melt to penetrate as in the transgranular cracks in Fig. 10. Alternatively, the presence of glass may reflect an anisotropy in the solid-liquid interfacial energy or a departure from textural equilibrium (Cooper and Kohlstedt, 1982).

Observations made with the phase-contrast technique support this conclusion. The pattern of Fresnel fringes in Fig. 8 is exactly the pattern expected in going from a region of high inner potential (the upper grain) to a region of lower inner potential (the lower grain) such as occurs in going from a solid grain into a hole (see for example, Thomas, Fig. 53, 1964). *If* there is an amorphous phase between the two crystalline grains in Fig. 8, its maximum thickness is ~1 nm, which is the width observed for the grain boundary region in the near-focus condition, Fig. 8c (Clarke 1979).

The 10nm wide bright band observed along the grain boundaries in the diffuse-scattering images (Fig. 7) cannot be correlated one-to-one with a glass layer. It is approximately ten times wider than the maximum possible width of a glass layer. Apparently, material is removed preferentially at the grain boundary during ion thinning. The resulting groove may then be filled with carbon when the sample is carbon coated to prevent charging in the electron beam. The carbon would then appear as an amorphous layer at the grain boundary to account for the anomalously wide bright band observed in the diffuse-scattering images (see also, Rühle et al. 1977).

Several triple junctions containing glass in the high pressure, long term samples have one crystallographically controlled solid-liquid interface. This interface is parallel to the (010) plane which also extends along the grain boundaries meeting at the triple junction. This geometry suggests anisotropy of surface energy of the solid-liquid interface and possibly anisotropy of the grain boundary energy. The latter is difficult to demonstrate since melt was probably present on the grain boundaries when they first formed. Surface energy anisotropy of the solid-liquid interface suggests that a truly equilibrium configuration does not require 120° grain intersections in systems such as olivine-basalt.

Summary and Conclusions

We have used transmission electron microscopy to study the fluid phase distribution, observed as glass in quenched specimens, in olivine-basalt assemblages in the absence of significant shear stresses. Samples which were hot pressed for short time durations have melt present along grain boundaries and lack the features characteristic of textural

equilibrium. In long duration runs in which textural equilibrium appears to be closely approached, virtually all of the glass phase is confined to intergranular triple junctions. Glass along grain boundaries, if indeed it exists, is less than 2 nm thick away from triple junctions except in the very small percentage of cases discussed above. This observation supports the thermodynamic model of Bulau et al. (1979) which predicts dry intergranular faces in equilibrium when olivine surface energies are isotropic. The triple junctions with an (010) crystal plane parallel to one side indicate a degree of crystallographically controlled anistropy in surface energy. The effect of this anisotropy on overall fluid geometry is small when crystalline grains are randomly oriented. However, it suggests the possibility of anisotropic fluid distribution and permeability in partial melts occurring within the mantle if olivine occurs with a strongly preferred orientation.

Direct application of the results presented here to the earth's mantle requires some speculative assumptions concerning the relevance of the somewhat different conditions. (1) The melt phase in parts of the upper mantle may have non-tholeiitic composition which might have different wetting properties. (2) Material in the mantle flows slowly under small deviatoric stresses which may influence the distribution of the melt phase. (3) Dynamic recrystallization may also play a role in continuously reorganizing the grain boundary structure. (4) The gravitational field will influence the wetting chracteristics of partial melts extended over large vertical distances (Waff 1982). Nevertheless, this study provides further insight into the nature of the equilibrium fluid distribution in silicate partial melts. An understanding of this distribution is needed for a realistic description of actual partial melts whithin the mantle.

Acknowledgements. The support of the National Science Foundation through Grants EAR 7919725 and EAR 8025725 is gratefully acknowledged. The electron microscopes used are part of the Cornell University Materials Science Center central facility for electron microscopy. J. Bulau helped with sample preparation, and D. Dimos carried out the SEM observations.

References

Bloss FD (1961) An introduction to the methods of optical crystallography. Holt, Rinehart and Winston, New York

Bulau JR, Waff HS, Tyburczy JA (1979) Mechanical and thermodynamic contraints on fluid distribution in partial melts. J Geophys Res 84:6102–6108

Clarke DR (1979) High-resolution techniques and application to nonoxide ceramics. J Am Ceram Soc 62:236–246

Clarke DR (1980) Observation of microcracks and thin intergranular films in ceramics by transmission electron microscopy. J Am Ceram Soc 63:104–106

Cooper RF, Kohlstedt DL (1982) Interfacial energies in the olivine-basalt system. In: Akimoto, S, Manghnani, MH, (eds) High-Pressure Research in Geophysics. Advances in Earth and Planetary Sciences vol. 12, Center for Academic Publications Japan. Tokyo, pp. 217–228

Cowley JM (1975) Diffraction physics. North-Holland, Amsterdam

Edington JW (1976) Practical electron microscopy in materials science. Van Nostrand Reinhold, New York

Kingery WD, Bower HK, Uhlmann DR (1976) Introduction to ceramics. Wiley & Sons, New York

Krivanek OL, Shaw TM, Thomas G (1979) Imaging of thin intergranular films by high resolution electron microscopy. J Appl Phys 50:4223–4227

Lou LKV, Mitchell TE, Heuer AH (1978) Impurity phases in hot-pressed Si_3N_4. Am Ceram Soc 61:392–396

Rühle M, Springer C, Gauckler LJ, Wilkens M (1977) TEM studies of phases in Si-Al-O-N alloys. In: Mura T, Hashimoto H (eds) Proceedings of the Fifth International Conference on high voltage electron microscopy. Japanese Society for Electron Microscopy, pp 641–644

Thomas G (1964) Transmission electron microscopy of metals. Wiley & Sons, New York

Waff HS (1980) Effects of the gravitational field on liquid distribution in partial melts within the upper mantle. J Geophys Res 85:1815–1825

Waff HS, Bulau JR (1979) Equilibrium fluid distribution in an ultramatic partial melt under hydrostatic stress conditions. J Geophys Res 84:6109–6114

Accepted August 9, 1982